Progress of Theoretical Physics, Vol. 106, No. 5, November 2001

Analyses of Type Ia Supernova Data in Cosmological Models with a Local Void

Kenji TOMITA*)

Yukawa Institute for Theoretical Physics, Kyoto University, Kyoto 606-8502, Japan

(Received August 3, 2001)

The data for type Ia supernovae obtained by the High-z SN Search Team and Supernova Cosmology Project are analyzed using inhomogeneous cosmological models with a local void on scales of about 200 Mpc, to derive the best-fit values of model parameters and the confidence contours. The χ^2 fitting is found to be slightly better than that in homogeneous models. It is shown that (1) the best-fit values are most sensitive to the ratio R of the outer Hubble constant, $H_0^{\rm II}$, to the inner Hubble constant, $H_0^{\rm I}$, (2) the best-fit outer density parameter, $\Omega_0^{\rm II}$, and cosmological constant parameter, $\lambda_0^{\rm II}$, are, respectively, increasing and decreasing functions of R, and (3) $(\Omega_0^{\rm II}, \lambda_0^{\rm II})$ can be $(1, 0)$ for $R \approx 0.8$. Moreover, it is shown that these models are naturally consistent with the new supernova data (SN1997ff) with $z = 1.7$.

§1. Introduction

In present day cosmology, the most important observations are those of the [magnitude m - redshift z] relation for type Ia supernovae (SNIa) and the CMB anisotropy. In the former observations, SNIa play the role of the best standard candles, and two groups, the High-z SN Search Team [1)-3)] and the Supernova Cosmology Project, [4)] have to this time observed 50 and 60 SNIa, respectively. Their results suggest that a significant amount of dark energy fills our universe, under the assumption of its homogeneity and isotropy.

Inhomogeneous models with a local void on scales of about 200 Mpc have been studied by the present author [5)] in connection with puzzling behavior of cosmic bulk flows [6),7)] and it was subsequently shown that it may be possible to explain the accelerating behavior of high-z SNIa in $[m, z]$ relation without a cosmological constant. [8)] A historical survey of works concerned with local voids is given in a previous work. [9)] Because these inhomogeneous models include many parameters (such as the inner and outer values of the Hubble constant and the density parameter, the cosmological constant, and the boundary radius), we recently examined the dependence of the above relation on these parameters, in comparison with the relations in homogeneous models with $(\Omega_0, \lambda_0) = (0.3, 0.7)$ and $(0.3, 0.0)$. [10)]

Observationally, recent galactic redshift surveys [11)-14)] show that in the region approximately $200 - 300h^{-1}$ Mpc from us, the distribution of galaxies may be inhomogeneous. Moreover, a large-scale inhomogeneity suggesting the existence of a wall around the void on scales of $\sim 250h^{-1}$ Mpc has recently been found by Blanton et al. [15)] from the SDSS commissioning data. Similar walls on scales of $\sim 250h^{-1}$

*) E-mail: tomita@yukawa.kyoto-u.ac.jp

Mpc have been found from the Las Campanas and 2dF redshift surveys near the Northern and Southern Galactic Caps.[16),13),17)] These results may imply that there is a local void of radius ~ 200 – $300h^{-1}$ Mpc in which we live.

In this paper we analyze directly the SNIa data of the above-mentioned two groups using our inhomogeneous models with a local void on scales of about 200 Mpc, and obtain the confidence contours as well as the best-fit values of the model parameters. In §2 we give the basic formulation of the distance modulus and the χ square for statistical fitting. In §3 we derive the best-fit values of model parameters and the confidence contours. In addition, we compare the behavior of our models with the new data for $z = 1.7$,[18)] and we find that they appear to be naturally consistent with it. In §4, discussion and concluding remarks are given.

§2. Distance modulus and the χ square

The theoretical distance modulus is defined by

$$\mu_0^p = 5 \log \left(d_{\rm L}/{\rm Mpc} \right) + 25, \tag{2·1}$$

where $d_{\rm L}$ is the luminosity distance, related to the angular-diameter distance $d_{\rm A}$ by

$$d_{\rm L} = (1+z)^2 d_{\rm A}, \tag{2·2}$$

along the light ray to a source S with redshift z. This distance modulus is compared with the observed one, given by

$$\mu_0 = m_B - M_B, \tag{2·3}$$

where M_B and m_B are the peak absolute magnitude and the corresponding apparent magnitude of a standard SNIa in the B band, respectively.

In this paper we consider spherical inhomogeneous cosmological models which consist of an inner homogeneous region, $\mathrm{V^I}$, and an outer homogeneous region, $\mathrm{V^{II}}$, with a boundary of radius ~ 200 Mpc. The observer's position O deviates generally from the center C, but is assumed to be close to C, compared with the boundary. For the off-center observer, the angular-diameter distance $d_{\rm A}$ depends not only on z, but also on the angle between the vectors $\overline{\rm CO}$ and $\overline{\rm CS}$, where S is the source. In our previous papers,[5),8)] the behavior of distances for off-center observers was studied. Since the angular dependence is small for remote sources, however, we can ignore it for simplicity, assuming that we are approximately at the center. Then $d_{\rm A}$ depends on the source redshift z, the inner and outer Hubble constants $H_0^{\rm I}$ and $H_0^{\rm II}$, the inner and outer density parameters $\Omega_0^{\rm I}$ and $\Omega_0^{\rm II}$, the outer Λ parameter $\lambda_0^{\rm II}$, and the boundary redshift z_1. The inner Λ parameter $\lambda_0^{\rm I}$ is related to $\lambda_0^{\rm II}$ by $\lambda_0^{\rm I} = \lambda_0^{\rm II}(H_0^{\rm II}/H_0^{\rm I})^2$. The equations to be solved to derive $d_{\rm A}$ and the junction conditions are Eqs. (5) – (11) in Ref. 10).

The best-fit values for the cosmological parameters are determined using the χ-square expression

$$\chi^2 = \sum_i \left[\mu_{0,i}^p(z_i | H_0^{\rm I}, H_0^{\rm II}, \Omega_0^{\rm I}, \Omega_0^{\rm II}, \lambda_0^{\rm II}, z_1) - \mu_{0,i} \right]^2$$

$$/(\sigma_{\mu 0,i}^2 + \sigma_{mz,i}^2), \tag{2·4}$$

where $\sigma_{\mu 0}$ is the measurement error of the distance modulus and σ_{mz} is the dispersion in the distance modulus corresponding to the dispersion of the galaxy redshift σ_z (coming from peculiar velocity and uncertainty). σ_{mz} is related to σ_z as

$$\sigma_{mz} = \frac{5}{\ln 10}\left(\frac{1}{d_{\rm L}}\frac{\partial d_{\rm L}}{\partial z}\right). \tag{2·5}$$

Next, the probability distribution function (PDF) must be obtained to derive the confidence contours and the most likely values of the model parameters. It is expressed as

$$p(H_0^{\rm I}, H_0^{\rm II}, \Omega_0^{\rm I}, \Omega_0^{\rm II}, \lambda_0^{\rm II}, z_1|\mu_0) \propto \exp\left(-\frac{1}{2}\chi^2\right), \tag{2·6}$$

which is consistent with Eq. (9) in Ref. 2).

In the present inhomogeneous models there are six parameters, and it is too complicated to consider all of them simultaneously. For this reason, we treat here several cases with specific values of $z_1, H_0^{\rm II}/H_0^{\rm I}$, and $\Omega_0^{\rm I}$. Then, the corresponding normalized PDF can be expressed as

$$\begin{aligned} &p(H_0^{\rm I}, \Omega_0^{\rm II}, \lambda_0^{\rm II}|\mu_0) \\ &= \frac{\exp(-\frac{1}{2}\chi^2)}{\int_{-\infty}^{\infty} dH_0^{\rm I} \int_{-\infty}^{\infty} d\lambda_0^{\rm II} \int_{\Omega_{0l}}^{\infty} \exp(-\frac{1}{2}\chi^2) d\Omega_0^{\rm II}} \end{aligned} \tag{2·7}$$

for given $z_1, H_0^{\rm II}/H_0^{\rm I}$, and $\Omega_0^{\rm I}$, where μ_0 is the set of distance moduli used and Ω_{0l} is the assumed lower limit of $\Omega_0^{\rm II}$, being 0 or $-\infty$. Physically, the region in which $\Omega_0^{\rm II} < 0$ is meaningless, although it is significant statistically. To obtain a probability distribution independent of $H_0^{\rm I}$, we can consider the following quantity:

$$p(\Omega_0^{\rm II}, \lambda_0^{\rm II}|\mu_0) = \int_{-\infty}^{\infty} p(H_0^{\rm I}, \Omega_0^{\rm II}, \lambda_0^{\rm II}|\mu_0) dH_0^{\rm I}. \tag{2·8}$$

The contours are determined by $p(\Omega_0^{\rm II}, \lambda_0^{\rm II}|\mu_0)$.

§3. Supernova data and the fitting

At present, we have two SNIa data sets to be used for determining cosmological parameters, that of HSST (Schmidt et al.,[1)] Riess et al.[2)]) with 50 SNIa and that of SCP (Perlmutter et al.[4)]) with 60 SNIa. 18 SNIa are common to both data. In the former, there are two types of μ_0 data, that due to the Multicolor Light Curve Shape method (MLCS) and that due to the template-fitting method. In each method, we can use the data for $z_i, \mu_{0,i}$ and $\sigma_{\mu 0,i}$ (with $i = 1$ – 50) given in their tables. Following Riess et al.[2)] for σ_z, we adopt $\sigma_z = 200$ km s^{-1} and add 2500 km s^{-1} in quadrature to σ_z for SNIa whose redshifts were determined from broad features in the SN spectrum.

In Ref. 4), the data for $m_{B,i}^{\rm eff}, z_i, \sigma_{mz,i}$ and $\sigma_{z,i}$ ($i = 1$ – 60) are given, but the values of $\mu_{0,i}$ were not published and are not available. As shown by Wang,[19)]

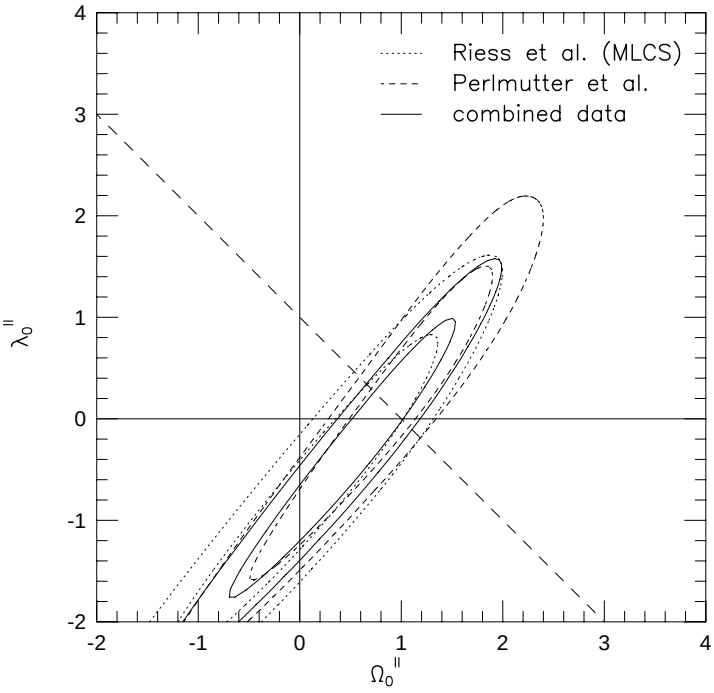

Fig. 1. The 68.3% and 95.4% confidence contours in the $\Omega_0^{\rm II}$ - $\lambda_0^{\rm II}$ plane in the case $(z_1, H_0^{\rm II}/H_0^{\rm I}, \Omega_0^{\rm I}) = (0.080, 0.82, {\rm A})$. The dotted curves represent the data of Riess et al. (1998), the dashed curves those of Perlmutter et al. (1999), and the solid curves the combined data.

however, we have for 18 SNIa observed by both teams

$$M_B^{\rm MLCS} \equiv m_B^{\rm eff} - \mu_0^{\rm MLCS} = -19.33 \pm 0.25, \tag{3·1}$$

where $m_B^{\rm eff}$ is the effective B-band magnitude of SNIa given by Perlmutter et al., and $\mu_0^{\rm MLCS}$ is the corresponding data for μ_0 due to MLCS method in Riess et al. [2)]

For the corrected B-band peak absolute magnitude derived by Hamuy et al., [20)] on the other hand, we have

$$M_B^{\rm MLCS} - M_B^{\rm H96} = -0.047 \pm 0.270, \tag{3·2}$$

which is sufficiently small, compared with the counterpart due to the template-fitting method. Accordingly, we adopt the MLCS data of Riess et al.'s two data sets, and derive the values of μ_0 from the data set of Perlmutter et al. using the relation

$$\mu_0 = m_B^{\rm eff} - \bar{M}_B \text{ with } \bar{M}_B = -19.33, \tag{3·3}$$

following Wang. [19)]

From the two data sets we make a combined data set consisting of 50 SNIa (from Riess et al.) and 42 SNIa (from Perlmutter et al.), in which we adopt the data of Riess et al. for 18 common data (due to Wang's procedure [19)]).

The above three kinds of data were compared with the theoretical models using the following conditions concerning $z_1, H_0^{\rm II}/H_0^{\rm I}$, and $\Omega_0^{\rm I}$. For z_1, we mainly used $z_1 =$

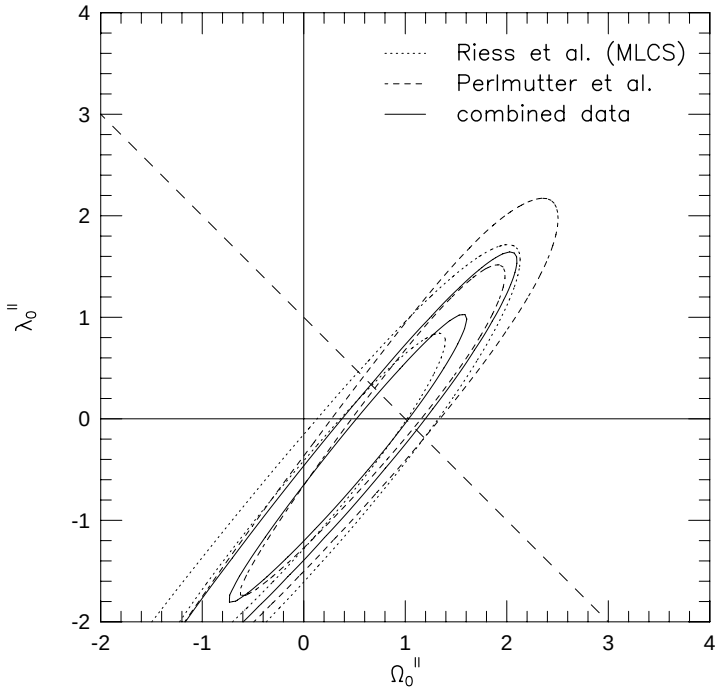

Fig. 2. The 68.3% and 95.4% confidence contours in the $\Omega_0^{\rm II}$ - $\lambda_0^{\rm II}$ plane in the case $(z_1, H_0^{\rm II}/H_0^{\rm I}, \Omega_0^{\rm I}) = (0.080, 0.82, {\rm B})$.

0.080, corresponding to the radius $240/h^{\rm I}$ Mpc, where $H_0^{\rm I} = 100h^{\rm I}$ km s^{-1} Mpc^{-1}. We compare the PDF in this case with the PDF in cases with $z_1 = 0.067$ ($cz_1/H_0^{\rm I} = 200/h^{\rm I}$ Mpc) and $z_1 = 0.100$ ($cz_1/H_0^{\rm I} = 300/h^{\rm I}$ Mpc) below. For $H_0^{\rm II}/H_0^{\rm I}$, we consider three cases, with $H_0^{\rm II}/H_0^{\rm I} = 0.80, 0.82$ and 0.87 (or $H_0^{\rm I}/H_0^{\rm II} = 1.25, 1.20$ and 1.15), respectively.

For $\Omega_0^{\rm I}$, we first consider the inner low-density case (A), in which

$$\Omega_0^{\rm I} = 0.3 \quad \text{for } \Omega_0^{\rm II} > 0.6 \tag{3·4}$$

and

$$\Omega_0^{\rm I} = \Omega_0^{\rm II}/2 \quad \text{for } \Omega_0^{\rm II} < 0.6. \tag{3·5}$$

For comparison, we also consider the equi-density case (B) with

$$\Omega_0^{\rm I} = \Omega_0^{\rm II} \left(H_0^{\rm II}/H_0^{\rm I} \right)^2. \tag{3·6}$$

Since $\rho_0^j \propto (H_0^j)^2 \Omega_0^j \quad (j = {\rm I}, {\rm II})$, we have $\rho_0^{\rm I} = \rho_0^{\rm II}$ in this case.

In Figs. 1 – 5, we plot the 68.3% and 95.4% confidence contours in the $\Omega_0^{\rm II}$ - $\lambda_0^{\rm II}$ plane. In Figs. 1, 2 and 3, we use three kinds of data and treat the three cases $(z_1, H_0^{\rm II}/H_0^{\rm I}, \Omega_0^{\rm I}) = (0.080,\ 0.82, {\rm A}),\ (0.080,\ 0.82, {\rm B}),$ and $(0.080, 0.82, {\rm A})$, with $\Omega_{0l} = 0$, respectively. Only in the case $\Omega_{0l} = 0$, the region of $\Omega_0^{\rm II} < 0$ is excluded. It is found comparing these figures that the difference between the two

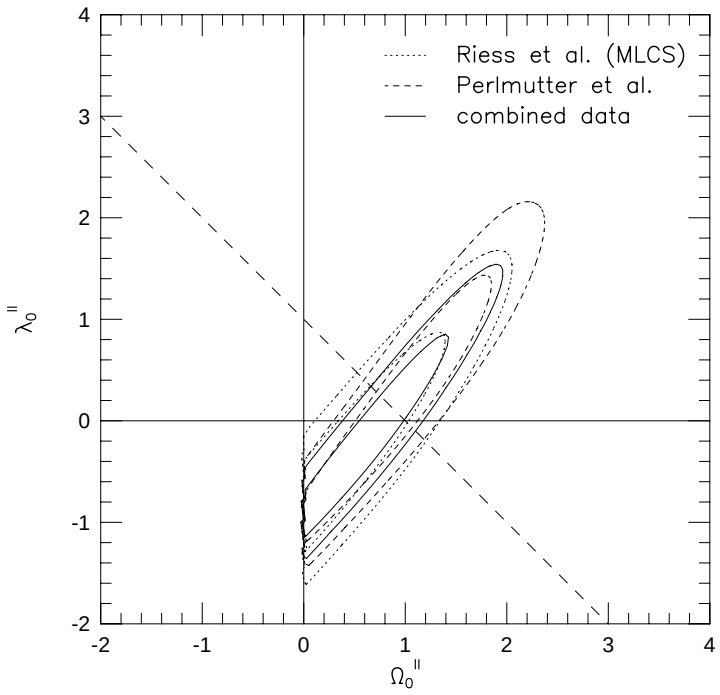

Fig. 3. The 68.3% and 95.4% confidence contours in the $\Omega_0^{\rm II}$ - $\lambda_0^{\rm II}$ plane in the case $(z_1, H_0^{\rm II}/H_0^{\rm I}, \Omega_0^{\rm I}) = (0.080, 0.82, {\rm A})$ with $\Omega_{0l} = 0$.

cases A and B is small, and the difference between the two cases with $\Omega_{0l} = -\infty$ and 0 is also small.

In Figs. 4 and 5, we display the difference between the contours in the cases $R \equiv H_0^{\rm II}/H_0^{\rm I} = 0.80,\ 0.82$ and 0.87 and $z_1 = 0.067,\ 0.080$ and 0.100, respectively, using the combined data. It is interesting that as R decreases, the contours move in the direction of increasing $\Omega_0^{\rm II}$ and decreasing $\lambda_0^{\rm II}$, and for $R = 0.80$, the flat case with vanishing cosmological constant (the Einstein-de Sitter model) is at the center of the contours.

In Table I, the best-fit values of the cosmological parameters in the homogeneous models are listed for later comparison. In Tables II, III and IV, we display the best-fit values of $h^{\rm I}, \Omega_0^{\rm II}$ and $\lambda_0^{\rm II}$ with 1σ error bars, and the corresponding values of χ_ν^2 in the cases $H_0^{\rm II}/H_0^{\rm I} = 0.82,\ 0.87$ and 0.80, respectively, assuming $z_1 = 0.080$ and $\Omega_0^{\rm I}$

Table I. Model parameters determined for the homogeneous models. Here, χ_ν^2 is the value of χ^2 per degree of freedom. $H_0 = 100h$ km s^{-1} Mpc^{-1}. The errors on h expressed here are only statistical.

data	Riess et al.	Perlmutter et al.	combined
h	0.65 ± 0.01	0.666 ± 0.02	0.65 ± 0.01
Ω_0	0.2 ± 0.6	1.0 ± 0.4	0.7 ± 0.4
λ_0	0.7 ± 0.8	1.7 ± 0.6	1.2 ± 0.5
χ_ν^2	1.11	1.57	1.45

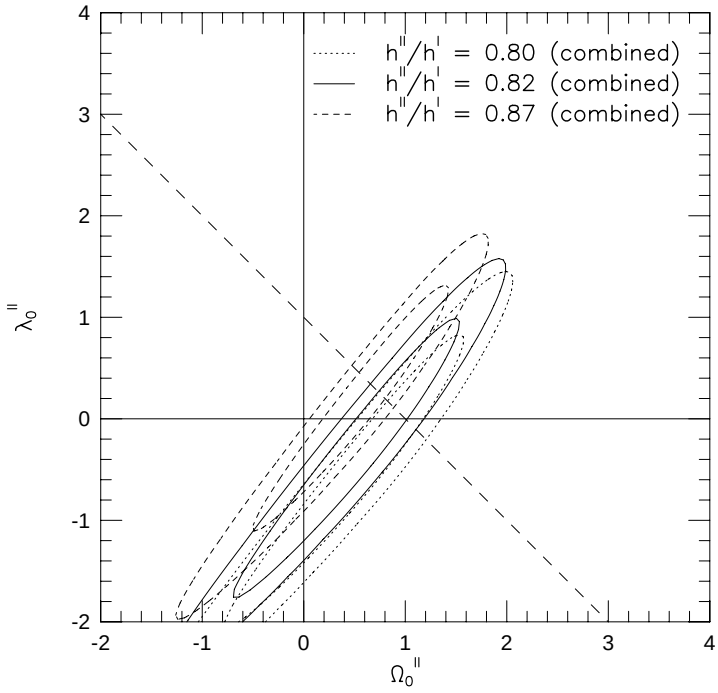

Fig. 4. The 68.3% and 95.4% confidence contours in the $\Omega_0^{\rm II}$ - $\lambda_0^{\rm II}$ plane for the combined data. The dotted curves, solid curves and dashed curves represent the cases $H_0^{\rm II}/H_0^{\rm I} = 0.80, 0.82$, and 0.87, respectively.

(A). The error bars on $h^{\rm I}$ include only statistical errors, not the contributions from the errors of the absolute magnitudes. The values of χ^2_ν for the data of Perlmutter et al. is found to be much larger than that for the data of Riess et al. This results from the situation that for Perlmutter et al. we made artificially the data for μ_0, using the average absolute magnitude. In the data of Riess et al., χ^2_ν in our inhomogeneous models is smaller than that in the homogeneous models (Table 1), and so these data seem to be fitted better by our inhomogeneous models or the inhomogeneity of Hubble constant, though more parameters are included in our case. To the bottom of Tables II – V, we add $(\Omega_0^{\rm II})_{\rm flat}$, the density parameter in the case that the outer region is spatially flat.

Table II. Model parameters determined in the case $(z_1, H_0^{\rm II}/H_0^{\rm I}, \Omega_0^{\rm I}) = (0.080, 0.80, {\rm A})$. χ^2_ν is the value of χ^2 per degree of freedom. $H_0^{\rm I} = 100h^{\rm I}$ km s^{-1} Mpc^{-1}. The errors on $h^{\rm I}$ are only statistical.

data	Riess et al.	Perlmutter et al.	combined
$h^{\rm I}$	0.64 ± 0.01	0.64 ± 0.02	0.64 ± 0.01
$\Omega_0^{\rm II}$	0.1 ± 0.7	0.9 ± 0.6	0.5 ± 0.5
$\lambda_0^{\rm II}$	-0.9 ± 1.0	-0.1 ± 0.8	-0.5 ± 0.7
χ^2_ν	1.05	1.62	1.42
$(\Omega_0^{\rm II})_{\rm flat}$	1.0 ± 0.2	1.0 ± 0.2	1.0 ± 0.1

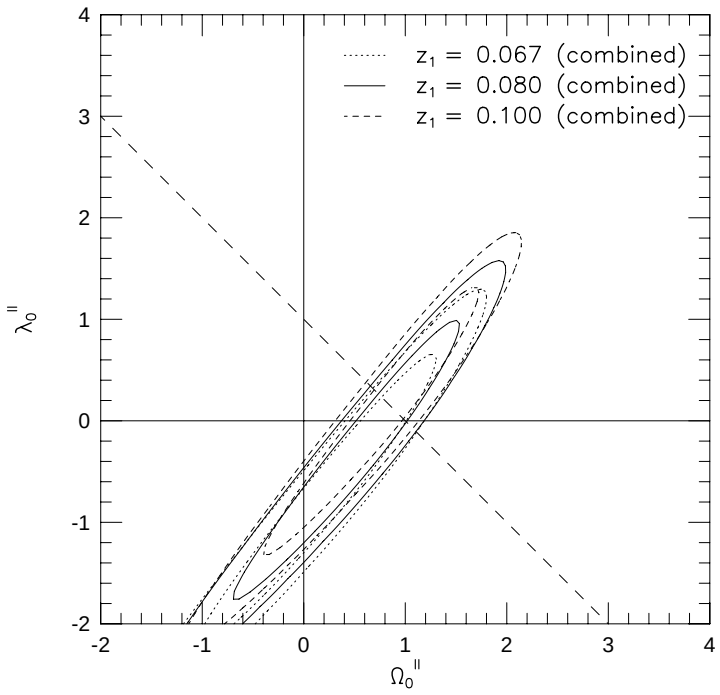

Fig. 5. The 68.3% and 95.4% confidence contours in the $\Omega_0^{\rm II}$ - $\lambda_0^{\rm II}$ plane for the combined data. The dotted curves, solid curves and dashed curves represent the cases $z_1 = 0.067, 0.080$, and 0.100, respectively.

In Table V we list the best-fit values in the case of $\Omega_0^{\rm I}$ (B), assuming $H_0^{\rm II}/H_0^{\rm I} = 0.82, z_1 = 0.080$. From a comparison of Tables II and V, we see that the best-fit values are not sensitive to $\Omega_0^{\rm I}$. In Table VI, moreover, we list the values for the cases with $z_1 = 0.067$ and 0.100, assuming $H_0^{\rm II}/H_0^{\rm I} = 0.82$ and $\Omega_0^{\rm I}$ (A). It is found from this table that, because of the smallest χ_ν^2, the fitting for $z_1 = 0.080$ is better than that in the cases with $z_1 = 0.067$ and 0.100. This result may be connected with the fact that the boundary radius of the observed local void is likely to be between $200/h^{\rm I}$ Mpc and $300/h^{\rm I}$ Mpc.

Finally, we compare the behavior of our models with the new supernova data for $z = 1.7$.[18] In Fig. 6 we show the $\Delta(m-M)$ - $\log z$ diagram, where $\Delta(m-M)$ is

Table III. Model parameters determined in the case $(z_1, H_0^{\rm II}/H_0^{\rm I}, \Omega_0^{\rm I}) = (0.080, 0.82, {\rm A})$. χ_ν^2 is the value of χ^2 per degree of freedom. $H_0^{\rm I} = 100h^{\rm I}$ km s^{-1} Mpc^{-1}. The errors on $h^{\rm I}$ are only statistical.

data	Riess et al.	Perlmutter et al.	combined
$h^{\rm I}$	0.64 ± 0.01	0.64 ± 0.02	0.64 ± 0.01
$\Omega_0^{\rm II}$	0.1 ± 0.7	0.9 ± 0.7	0.6 ± 0.5
$\lambda_0^{\rm II}$	-0.7 ± 1.1	0.1 ± 1.0	-0.2 ± 0.7
χ_ν^2	1.05	1.61	1.42
$(\Omega_0^{\rm II})_{\rm flat}$	0.9 ± 0.2	0.9 ± 0.2	0.9 ± 0.1

Table IV. Model parameters determined for the case $(z_1, H_0^{\rm II}/H_0^{\rm I}, \Omega_0^{\rm I}) = (0.080, 0.87, {\rm A})$. χ_ν^2 is the value of χ^2 per degree of freedom. $H_0^{\rm I} = 100h^{\rm I}$ km s^{-1} Mpc^{-1}. The errors on $h^{\rm I}$ are only statistical.

data	Riess et al.	Perlmutter et al.	combined
$h^{\rm I}$	0.64 ± 0.01	0.65 ± 0.02	0.64 ± 0.01
$\Omega_0^{\rm II}$	0.2 ± 1.0	0.7 ± 0.7	0.6 ± 0.6
$\lambda_0^{\rm II}$	-0.2 ± 1.1	0.7 ± 1.1	0.3 ± 0.8
χ_ν^2	1.05	1.61	1.42
$(\Omega_0^{\rm II})_{\rm flat}$	0.7 ± 0.2	0.7 ± 0.2	0.7 ± 0.1

Table V. Model parameters determined for the case $(z_1, H_0^{\rm II}/H_0^{\rm I}, \Omega_0^{\rm I}) = (0.080, 0.82, {\rm B})$. χ_ν^2 is the value of χ^2 per degree of freedom. $H_0^{\rm I} = 100h^{\rm I}$ km s^{-1} Mpc^{-1}. The errors on $h^{\rm I}$ are only statistical.

data	Riess et al.	Perlmutter et al.	combined
$h^{\rm I}$	0.64 ± 0.01	0.64 ± 0.02	0.64 ± 0.01
$\Omega_0^{\rm II}$	0.0 ± 0.7	0.8 ± 0.7	0.5 ± 0.5
$\lambda_0^{\rm II}$	-0.8 ± 1.1	0.0 ± 1.0	-0.3 ± 0.8
χ_ν^2	1.05	1.62	1.42
$(\Omega_0^{\rm II})_{\rm flat}$	0.9 ± 0.2	0.9 ± 0.2	0.9 ± 0.1

Table VI. Model parameters determined for the case $(z_1, H_0^{\rm II}/H_0^{\rm I}, \Omega_0^{\rm I}) = (0.080, 0.82, {\rm A})$. χ_ν^2 is the value of χ^2 per degree of freedom. $H_0^{\rm I} = 100h^{\rm I}$ km s^{-1} Mpc^{-1}. The errors on $h^{\rm I}$ are only statistical.

data	Riess et al.	Riess et al.	combined	combined
z_1	0.067	0.100	0.067	0.100
$h^{\rm I}$	0.64 ± 0.01	0.64 ± 0.01	0.64 ± 0.01	0.64 ± 0.01
$\Omega_0^{\rm II}$	-0.3 ± 0.7	0.4 ± 0.7	0.2 ± 0.5	0.9 ± 0.5
$\lambda_0^{\rm II}$	-1.3 ± 1.1	-0.3 ± 1.1	-0.7 ± 0.8	0.2 ± 0.8
χ_ν^2	1.10	1.13	1.45	1.46

the difference between $m - M$ in each model and that in the empty homogeneous model ($\Omega_0 = \lambda_0 = 0$). Here we have adopted two models with a local void in which $(\Omega_0^{\rm II}, \lambda_0^{\rm II}) = (1.0, 0.0)$ and $(0.6, 0.0)$. In both models we use $\Omega_0^{\rm I} = 0.3$, $\lambda_0^{\rm I} = 0$ and $z_1 = 0.067$ as the other parameters, to which the behavior of the models is not sensitive. The upper, middle and lower curves in each model correspond to R ($\equiv H_0^{\rm II}/H_0^{\rm I}$) $= 0.80, 0.82$ and 0.87, respectively. For comparison, we also display the behavior of three homogeneous models with $(\Omega_0, \lambda_0) = (0.35, 0.65), (0.35, 0.0)$ and $(1.0, 0.0)$, and depict in the diagram the binned data ($z < 1$) and the new data (SN 1997ff) for $z = 1.7$, which are given in Fig. 11 of Ref. 18). It is found from Fig. 6 that our models can be consistent with the new data, in contrast to the flat homogeneous model with $(\Omega_0, \lambda_0) = (0.35, 0.65)$. In particular, the model with $(\Omega_0^{\rm II}, \lambda_0^{\rm II}) = (1.0, 0.0)$, which is the Einstein-de Sitter model in the external region, seems to naturally accord with all data with $R = 0.80$ and 0.82. In the model with $(\Omega_0^{\rm II}, \lambda_0^{\rm II}) = (0.6, 0.0)$, the case $R = 0.87$ is best among the three cases. If more data for $z > 1$ are provided, we shall be able to distinguish more clearly the behavior of the models with a local void and that of the homogeneous models with dominant cosmological constant or dark energy.

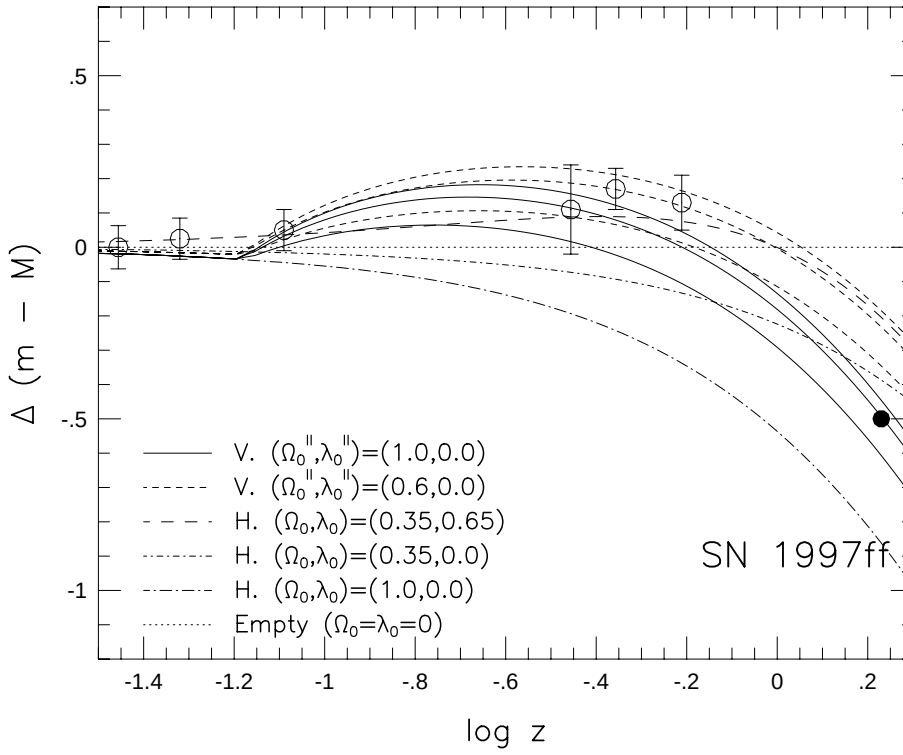

Fig. 6. The $\Delta(m-M)$ - $\log z$ diagram for models with a local void (V) and homogeneous models (H). Here $\Delta(m-M) \equiv (m-M)$ in each model $-$ $(m-M)$ in the empty model ($\Omega_0 = \lambda_0 = 0$). In the two V models, we have upper, middle and lower curves corresponding to $R\ (\equiv H_0^{\rm II}/H_0^{\rm I}) = 0.80, 0.82$ and 0.87, respectively. For comparison, the SNIa binned data ($z < 1$) and the new data for SN 1997ff ($z = 1.7$) are also depicted in the diagram.

§4. Concluding remarks

In this paper we derived confidence contours and best-fit parameters for inhomogeneous models with a local void using two sets of SNIa data and the combined data, and we found that (1) they are very sensitive to the ratio R of the outer Hubble constant $H_0^{\rm II}$ to the inner Hubble constant $H_0^{\rm I}$, (2) the best-fit outer density parameter $\Omega_0^{\rm II}$ increases and the cosmological constant parameter $\lambda_0^{\rm II}$ decreases as functions of R, and (3) $(\Omega_0^{\rm II}, \lambda_0^{\rm II})$ can be $(1, 0)$ for $R \approx 0.8$. It is thus found that the existence of our local void may solve the puzzling *cosmological-constant* problem.

However, we ignored the directional dependence of the $[m, z]$ relation, which may be an important factor, especially for nearby SNIa, since magnitudes of SNIa are measured by off-center observers. If the data of angular positions of observed SNIa are published, it should be possible to take into account the directional dependence, and the fitting may be improved.

The flux averaging proposed by Wang [19] was not carried out here, but it may be important when many high-z data with $z > 1.0$ appear, because they would be much affected by the lensing effect.

From a comparison with the new data for $z = 1.7$, we found that our models are naturally cosnsistent with it, in contrast to the homogeneous models with acceleration due to the cosmological constant or dark energy. For $z > 1$, the behavior of curves represents the deceleration of the universe, which depends strongly on the equation of state of the constituent matter. In our models with a local void, this is mainly pressureless matter, while the homogeneous models with the dominant cosmological constant and hypothetical dark energy have negative pressure comparable with the mass energy. More data with $z > 1.5$ is needed in order to distinguish these two types of models more clearly and remove the fluctuations due to the lensing effect.

Acknowledgements

The author is grateful to referees for helpful comments. This work was supported by a Grant-in Aid for Scientific Research (No. 12440063) from the Ministry of Education, Science, Sports and Culture, Japan. He owes also to the YITP computer system for the numerical analyses.

References

1) B. P. Schmidt, N. B. Suntzeff, M. M. Pillips, R. A. Schommer, A. Clocchiatti, R. P. Kirshner, P. Garnavich, P. Challis et al., Astrophys. J. **507** (1998), 46.
2) A. G. Riess, A. V. Filippenko, P. Challis, A. Clocchiatti, A. Diercks, P. M. Garnavich, R. L. Gilliland et al., Astron. J. **116** (1998), 1009.
3) A. G. Riess, A. V. Filippenko, W. Li and B. Schmidt, Astron. J. **118** (2000), 2668.
4) S. Perlmutter, G. Aldering, G. Goldhaber, R. A. Knop, P. Nugent, D. E. Groom, P. G. Castro, S. Deustua et al., Astrophys. J. **517** (1999), 565.
5) K. Tomita, Astrophys. J. **529** (2000), 26
6) M. J. Hudson, R. J. Smith, J. R. Lucey, D. J. Schlegel and R. L. Davies, Astrophys. J. **512** (1999), L79.
7) J. A. Willick, Astrophys. J. **522** (1999), 647.
8) K. Tomita, Astrophys. J. **529** (2000), 38.
9) K. Tomita, Prog. Theor. Phys. **105** (2001), 419, astro-ph/0005031.
10) K. Tomita, Mon. Not. R. Astron. Soc. **326** (2001), 287.
11) C. Marinoni, P. Monaco, G. Giuricin and B. Costantini, Astrophys. J. **521** (1999), 50.
12) R. O. Marzke, L. N. da Costa, P. S. Pellegrini, C. N. A. Willmer and M. J. Geller, Astrophys. J. **503** (1998), 617.
13) S. Folkes, S. Ronen, I. Price, O. Lahav, M. Colless, S. Maddox, K. Deeley, K. Glazebrook et al., Mon. Not. R. Astron. Soc. **308** (1999), 459.
14) E. Zucca, G. Zamorani, G. Vettolani, A. Cappi, R. Merighi, M. Mignoli, H. MacGillivray, C. Collins et al., Astron. Astrophys. **326** (1997), 477.
15) M. R. Blanton, J. Dalcanton, J. Eisenstein, J. Loveday, M. A. Strauss, M. SubbaRau, D. H. Weinberg, J. E. Anderson, Jr. et al., Astron. J. **121** (2001), 2358.
16) S. A. Shectman, S. D. Landy, A. Oemler, D. L. Tucker, H. Lin, R. P. Kirshner and P. L. Schecter, Astrophys. J. **470** (1996), 172.
17) S. Cole, P. Norberg, C. M. Baugh, C. S. Frenk, J. Bland-Hawthorn, T. Bridges, R. Cannon and M. Colless, Mon. Not. R. Astron. Soc. **326** (2001), 255.
18) A. G. Riess et al., astro-ph/0104455.
19) Y. Wang, Astrophys. J. **536** (2000), 531.
20) M. Hamuy et al., Astron. J. **112** (1996), 239.